2582 *Chem. Mater.* **2010,** *22,* 2582–2587
DOI:10.1021/cm903733s

CHEMISTRY OF MATERIALS
Article

Layer-by-Layer Assembly of TaO_3 Nanosheet/Polycation Composite Nanostructures: Multilayer Film, Hollow Sphere, and Its Photocatalytic Activity for Hydrogen Evolution

Jianhua Huang,[†,‡] Renzhi Ma,[†] Yasuo Ebina,[†] Katsutoshi Fukuda,[†] Kazunori Takada, and Takayoshi Sasaki*[,†]

[†]*International Center for Materials Nanoarchitectonics (MANA), National Institute for Materials Science (NIMS), 1-1 Namiki, Tsukuba, Ibaraki 305-0044, Japan, and* [‡]*Department of Chemistry, Zhejiang Sci-Tech University, Hangzhou 310018, People's Republic of China*

Received December 12, 2009. Revised Manuscript Received February 16, 2010

Multilayer composite films comprising of TaO_3 nanosheet crystallites and poly(diallyldimethylammonium chloride) (PDDA) were assembled via layer-by-layer sequential adsorption. Exposure of the resulting films to UV light promoted photocatalytic decomposition of PDDA in the nanosheet gallery to yield inorganic films. Novel hollow microspheres of Ta_2O_5 were fabricated by the deposition of a PDDA/TaO_3 multilayer nanoshell on polystyrene (PS) beads and the subsequent removal of the PS core and PDDA layers via calcination. The hollow microspheres showed photocatalytic properties effective for hydrogen evolution from an aqueous methanol solution. The shape control into hollow microsphere greatly enhanced the photocatalytic activity. The results highlight the role of the surface area and crystallinity of the catalyst in photocatalytic activity.

Introduction

Tantalum oxide has a variety of superior properties including good chemical resistance and a high melting point. It is a typical semiconducting material with a wide bandgap of ~3.9 eV, exhibiting photocatalytic properties. Attempts to enhance the photocatalytic activity of tantalum oxide have focused on the synthesis of its various forms, and Ta_2O_5 nanostructures such as nanotubes and nanodots have been obtained.[1,2]

Kominami et al. synthesized Ta_2O_5 nanoparticles through a solvothermal reaction of tantalum pentabutoxide in toluene. They found that Ta_2O_5 nanoparticles performed at a level about 10-fold higher than that of commercial Ta_2O_5 powder for H_2 evolution from an aqueous 2-propanol solution.[3] Nanosized-Ta_2O_5 powder photocatalyst was also prepared via the sol−gel method using $TaCl_5$ as a precursor, and the photocatalytic activity proved effective for the degradation of gaseous formaldehyde under UV irradiation. The calcination temperature and time were found to play an important role in determining the crystal structure and photocatalytic activity of Ta_2O_5 powder.[4] A recent study reported approximately 7 times higher activity of crystallized mesoporous Ta_2O_5 compared to that of commercial Ta_2O_5 powder, where mesoporous Ta_2O_5 photocatalyst was synthesized through a surfactant-assisted sol−gel process.[5] Moreover, mesoporous Ta_2O_5 loaded with cocatalysts showed high photocatalytic activity for the production of H_2 and O_2 from overall water splitting.[6,7] Ta_2O_5 hollow spheres were recently prepared through the surface precipitation of Ta_2O_5 on β-diketone-functionalized polystyrene (PS) beads by hydrolyzing tantalum ethoxide and subsequent calcination.[8] Hollow spheres, in general, have lower density, greater surface area and higher surface permeability compared to corresponding bulk materials. Accordingly, good photocatalytic activities are expected in them. However, the Ta_2O_5 hollow spheres reported have a fairly large shell thickness of several hundreds of nanometers, and their photocatalytic properties have not yet been reported.

Apart from the photocatalytic activities, because of high dielectric constant, large refractive index value, as well as high chemical and thermal stability, Ta_2O_5 films involve various applications,[9] such as for antireflective layers in optical devices,[10] dielectric layers for storage

*Corresponding author. E-mail: sasaki.takayoshi@nims.go.jp.

(1) Allam, N. K.; Feng, X. J.; Grimes, C. A. *Chem. Mater.* **2008**, *20*, 6477.
(2) Wu, C.-T.; Ko, F.-H.; Hwang, H.-Y. *Microelectron. Eng.* **2006**, *83*, 1567.
(3) Kominami, H.; Miyakawa, M.; Murakami, S.; Yasuda, T.; Kohno, M.; Onoue, S.; Kera, Y.; Ohtani, B. *Phys. Chem. Chem. Phys.* **2001**, *3*, 2697.
(4) Zhu, Y.; Yu, F.; Man, Y.; Tian, Q.; He, Y.; Wu, N. *J. Solid State Chem.* **2005**, *178*, 224.
(5) Sreethawong, T.; Ngamsinlapasathian, S.; Suzuki, Y.; Yoshikawa, S. *J. Mol. Catal. A: Chem.* **2005**, *235*, 1.
(6) Noda, Y.; Lee, B.; Domen, K.; Kondo, J. N. *Chem. Mater.* **2008**, *20*, 5361.
(7) Takahara, Y.; Kondo, J. N.; Takata, T.; Lu, D.; Domen, K. *Chem. Mater.* **2001**, *13*, 1194.
(8) Agrawal, M.; Pich, A.; Gupta, S.; Zafeiropoulos, N. E.; Simon, P.; Stamm, M. *Langmuir* **2008**, *24*, 1013.
(9) Chaneliere, C.; Autran, J. L.; Devine, R. A. B.; Balland, B. *Mater. Sci. Eng., R* **1998**, *22*, 269.
(10) Rehg, T. J.; Ochoa-Tapia, J. A.; Knoesen, A.; Higgins, B. G. *Appl. Opt.* **1989**, *28*, 5215.

Published on Web 03/08/2010

capacitors in dynamic random access memories (DRAMs) and metal-oxide-semiconductor (MOS) devices,[11] dielectric layers in biological sensors,[12] and insulating layers in thin-film electroluminescent devices.[13] Therefore, fabrication of high-quality thin films of Ta_2O_5 and related oxides is of significant importance.

In the past dacades, delamination of layered host compounds has attracted much attention, because resulting colloidal single layers can be taken as a unique class of two-dimensional nanoscale materials.[14−23] The nanosheet crystallites have a thickness of 0.5−3 nm and a lateral size of micrometers range, meaning that they are composed entirely of surface atoms arranged two-dimensionally in a single-crystal-like order. Such nanosheets can be assembled layer-by-layer into ordered multilayer films using the sequential adsorption method.[17b,c,24] Meanwhile, because the nanosheets are flexible enough to smoothly coat the curved surface, core−shell composites can be fabricated using the nanosheets as a shell building block.[24f,25] The thickness of the films and shells can be finely controlled in steps of nanosheet thickness, that is ~1 nm. Although the resultant hollow microspheres fabricated with semiconducting titania nanosheet are attractive and promising as a photocatalyst, their photocatalytic properties have never been investigated. Recently, we have reported successful delamination of layered $RbTaO_3$ into colloidal TaO_3 nanosheet crystallites.[26] It is of great interest to fabricate nanostructured materials using TaO_3 nanosheet as a building block and explore their properties.

In the current work, we fabricated multilayer composite films of exfoliated TaO_3 nanosheets and polycation using the alternate adsorption technique. Their photocatalytic degradation ability of organic materials was examined. Core−shell composites were successfully prepared by similar adsorption procedures of polycation and TaO_3 nanosheets onto the surface of PS beads, which were then converted into inorganic hollow microspheres by calcination. The hollow spheres were found to undergo a high hydrogen gas generation from an aqueous methanol solution.

Experimental Section

Synthesis of TaO_3 Nanosheet. Reagents, such as Ta_2O_5, Rb_2CO_3 and NaCl, were of >99.9% purity or of analytical grade. Poly(diallyldimethylammonium chloride) (PDDA) was purchased from Aldrich Chemical Co. PS beads with an average diameter of 1.3 μm were a gift from Soken Chemical Co. and used as received. Ultrapure water (>17 MΩ cm) from a Milli-Q water system was used throughout the experiments. A colloidal suspension of exfoliated TaO_3 nanosheets was synthesized according to the previously reported method.[26] The starting layered material of $RbTaO_3$ was prepared by heating a mixture of Ta_2O_5 and Rb_2CO_3 at 900 °C for 20 h. This was converted into protonic oxide, $Rb_{0.1}H_{0.9}TaO_3 \cdot 1.3H_2O$, by repeating acid-exchange several times using 1 mol dm^{-3} HCl solution. Colloidal TaO_3 nanosheets were obtained by shaking the protonated sample in a tetrabutylammonium hydroxide (TBAOH) solution for 2 weeks.

Layer-by-Layer Assembly into Multilayer Films. Substrates, such as Si wafers and quartz glass slides, were cleaned using acetone, followed by treatment in a bath of methanol/HCl (1:1 in volume) and then concentrated H_2SO_4 for 30 min each. Multilayer films were fabricated by applying the sequential adsorption method.[24] The substrate was first immersed in a PDDA solution (20 g dm^{-3}, pH 9.0) for 20 min. After being washed thoroughly with pure water, the PDDA-coated substrate was dipped into a colloidal suspension of TaO_3 nanosheet (0.08−0.30 g dm^{-3}, pH 9.0) for 20 min, followed by washing with copious water. The above procedure was repeated n times to obtain multilayer films of $(PDDA/TaO_3)_n$.

Fabrication of Core−Shell Composites and Hollow Spheres. A typical procedure for the layer-by-layer deposition of PDDA

(11) Paskaleva, A.; Tapajna, M.; Atanassova, E.; Frohlich, K.; Vincze, A.; Dobročka, E. *Appl. Surf. Sci.* **2008**, *254*, 5879.
(12) Gebbert, A.; Alvarez-Icaza, M.; Stöcklein, W.; Schmid, R. D. *Anal. Chem.* **1992**, *64*, 997.
(13) Kukli, K.; Ihanus, J.; Ritala, M.; Leskela, M. *Appl. Phys. Lett.* **1996**, *68*, 3737.
(14) Sasaki, T. *J. Ceram. Soc. Jpn.* **2007**, *115*, 9.
(15) (a) Sasaki, T.; Watanabe, M.; Hashizume, H.; Yamada, H.; Nakazawa, H. *J. Am. Chem. Soc.* **1996**, *118*, 8329. (b) Sasaki, T.; Watanabe, M. *J. Am. Chem. Soc.* **1998**, *120*, 4682. (c) Tanaka, T.; Ebina, Y.; Takada, K.; Kurashima, K.; Sasaki, T. *Chem. Mater.* **2003**, *15*, 3564. (d) Sugimoto, W.; Terabayashi, O.; Murakami, Y.; Takasu, Y. *J. Mater. Chem.* **2002**, *12*, 3814. (e) Miyamoto, N.; Kuroda, K.; Ogawa, M. *J. Mater. Chem.* **2004**, *14*, 165.
(16) (a) Miyamoto, N.; Yamamoto, H.; Kaito, R.; Kuroda, K. *Chem. Commun.* **2002**, 2378. (b) Takagaki, A.; Lu, D.; Kondo, J. N.; Hara, M.; Hayashi, S.; Domen, K. *Chem. Mater.* **2005**, *17*, 2487. (c) Takagaki, A.; Yoshida, T.; Lu, D.; Kondo, J. N.; Hara, M.; Domen, K.; Hayashi, S. *J. Phys. Chem. B* **2004**, *108*, 11549.
(17) (a) Treacy, M. M. J.; Rice, S. B.; Jacobson, A. J.; Lewandowski, J. T. *Chem. Mater.* **1990**, *2*, 279. (b) Fang, M.; Kim, C. H.; Saupe, G. B.; Kim, H.-N.; Waraksa, C. C.; Miwa, T.; Fujishima, A.; Mallouk, T. E. *Chem. Mater.* **1999**, *11*, 1526. (c) Schaak, R. E.; Mallouk, T. E. *Chem. Mater.* **2000**, *12*, 2513. (d) Ozawa, T. C.; Fukuda, K.; Akatsuka, K.; Ebina, Y.; Sasaki, T. *Chem. Mater.* **2007**, *19*, 6575. (e) Ida, S.; Ogata, C.; Eguchi, M.; Youngblood, W. J.; Mallouk, T. E.; Matsumoto, Y. *J. Am. Chem. Soc.* **2008**, *130*, 7052.
(18) (a) Liu, Z.-H.; Ooi, K.; Kanoh, H.; Tang, W. P.; Tomida, T. *Langmuir* **2000**, *16*, 4154. (b) Gao, Q.; Giraldo, O.; Tong, W.; Suib, S. L. *Chem. Mater.* **2001**, *13*, 778. (c) Omomo, Y.; Sasaki, T.; Wang, L. Z.; Watanabe, M. *J. Am. Chem. Soc.* **2003**, *125*, 3568. (d) Liu, Z.; Ma, R.; Ebina, Y.; Takada, K.; Sasaki, T. *Chem. Mater.* **2007**, *19*, 6504.
(19) (a) Schaak, R. E.; Mallouk, T. E. *Chem. Commun.* **2002**, 706. (b) Fukuda, K.; Akatsuka, K.; Ebina, Y.; Ma, R.; Takada, K.; Nakai, I.; Sasaki, T. *ACS Nano* **2008**, *2*, 1689.
(20) Sugimoto, W.; Iwata, H.; Yasunaga, Y.; Murakami, Y.; Takasu, Y. *Angew. Chem., Int. Ed.* **2003**, *42*, 4092.
(21) Nakato, T.; Furumi, Y.; Terao, N.; Okuhara, T. *J. Mater. Chem.* **2000**, *10*, 737.
(22) (a) Adachi-Pagano, M.; Forano, C.; Besse, J.-P. *Chem. Commun.* **2000**, 91. (b) Hibino, T.; Jones, W. *J. Mater. Chem.* **2001**, *11*, 1321. (c) Li, L.; Ma, R.; Ebina, Y.; Iyi, N.; Sasaki, T. *Chem. Mater.* **2005**, *17*, 4386. (d) Liu, Z.; Ma, R.; Osada, M.; Iyi, N.; Ebina, Y.; Takada, K.; Sasaki, T. *J. Am. Chem. Soc.* **2006**, *128*, 4872.
(23) (a) Lee, B.-I.; Lee, K. S.; Lee, J. H.; Lee, I. S.; Byeon, S.-H. *Dalton Trans.* **2009**, 2490. (b) Hu, L.; Ma, R.; Ozawa, T. C.; Sasaki, T. *Chem. Asian J.* **2010**, *5*, 248.
(24) (a) Kleinfeld, E. R.; Ferguson, G. S. *Science* **1994**, *265*, 370. (b) Lvov, Y.; Ariga, K.; Ichinose, I.; Kunitake, T. *Langmuir* **1996**, *12*, 3038. (c) Keller, S. W.; Kim, H.-N.; Mallouk, T. E. *J. Am. Chem. Soc.* **1994**, *116*, 8817. (d) Kotov, N. A.; Haraszti, T.; Turi, L.; Zavala, G.; Geer, R. E.; Dékány, I.; Fendler, J. H. *J. Am. Chem. Soc.* **1997**, *119*, 6821. (e) Sasaki, T.; Ebina, Y.; Tanaka, T.; Harada, M.; Watanabe, M.; Decher, G. *Chem. Mater.* **2001**, *13*, 4661. (f) Wang, L. Z.; Ebina, Y.; Takada, K.; Sasaki, T. *J. Phys. Chem. B* **2004**, *108*, 4283. (g) Tanaka, T.; Fukuda, K.; Ebina, Y.; Takada, K.; Sasaki, T. *Adv. Mater.* **2004**, *16*, 872.
(25) (a) Wang, L. Z.; Sasaki, T.; Ebina, Y.; Kurashima, K.; Watanabe, M. *Chem. Mater.* **2002**, *14*, 4827. (b) Wang, L. Z.; Ebina, Y.; Takada, K.; Sasaki, T. *Chem. Commun.* **2004**, 1074. (c) Li, L.; Ma, R.; Iyi, N.; Ebina, Y.; Takada, K.; Sasaki, T. *Chem. Commun.* **2006**, 3125.
(26) Fukuda, K.; Nakai, I.; Ebina, Y.; Ma, R.; Sasaki, T. *Inorg. Chem.* **2007**, *46*, 4787.

and TaO_3 nanosheets on the PS surface was performed as follows: 0.30 g of PS beads was dispersed in 100 cm^3 of aqueous solution containing 20 g dm^{-3} PDDA and 0.15 mol dm^{-3} NaCl (pH 9.0) under stirring. The mixture was ultrasonically treated for 10 min to homogeneously disperse the PS beads and then further stirred for another 15 min to ensure the saturated adsorption of PDDA on the PS surface. Excess PDDA was removed by twice-repeated centrifugation (6000 rpm, 10 min) and water washing. The recovered PS particles coated with PDDA were redispersed in 100 cm^3 of pure water, followed by ultrasonic treatment for another 10 min to avoid possible aggregation of particles. Then, 5 cm^3 of the colloidal suspension of TaO_3 nanosheets (8 g dm^{-3}) were added drop by drop under stirring. The particles were collected by twice-repeated centrifugation (6000 rpm, 10 min) and water washing. Core−shell composites coated with n bilayers of PDDA/TaO_3 were fabricated by repeating the above procedure n times.

To obtain hollow spheres, the core−shell composites were heated to 600 °C in air at a heating rate of 20 °C h^{-1} and held them at this temperature for 4 h to fully combust the PS core and PDDA layers.

Characterization. The surface topography of the films was examined using a Seiko SPA400 atomic force microscope (AFM) in tapping mode with a silicon-tip cantilever (15 N m^{-1}). Ultraviolet−visible (UV−vis) absorption spectra were recorded using a Hitachi U-4100 spectrophotometer. X-ray diffraction (XRD) data were collected by a Rigaku Rint 2000 powder diffractometer with monochromatized CuKα radiation (λ = 0.15405 nm). Morphology of samples was examined using a JEOL JSM-5800LV scanning electron microscope (SEM) operated at 2 or 5 kV. A JEOL 3000F transmission electron microscope (TEM) operated at 300 kV was employed to obtain TEM images and selected area electron diffraction (SAED) patterns. Thermogravimetric measurements (TG-DTA) were carried out using a Rigaku TG-8120 instrument. Nitrogen adsorption−desorption isotherms were measured using a Quantachrome instrument, AUTOSORB-1.

Photocatalytic Reaction. Tests of photocatalytic hydrogen generation from an aqueous methanol solution were performed as follows: 1.0 mg catalyst was suspended in 2.0 cm^3 of aqueous 10 vol % methanol solution in a quartz reaction cell (3.5 cm^3 capacity), which was placed in an outer jacket and sealed with PTFE sealing tape. The reaction cell was purged with Ar gas for 15 min, after which an Ar gas flow was introduced into the outer jacket to prevent air contamination during the photocatalytic reaction. The dispersion, under constant stirring, was irradiated using a UV light source (500W Xe lamp, San-ei Electric Co., Ltd.). Throughout the reaction, a headspace gas sample (0.1 cm^3) was collected by syringe every hour. Hydrogen content in the gas sample was analyzed by gas chromatography (Shimadzu GC-14, MS-5A column, Ar carrier, TCD).

Commercial Ta_2O_5 powder (99.9%, orthorhombic phase, purchased from Rare Metallic Co., Ltd.) was utilized for comparative photocatalytic experiments.

Results and Discussion

Characterization of the TaO_3 Nanosheet. Both the starting material $RbTaO_3$ and its protonic oxide $Rb_{0.1}H_{0.9}TaO_3 \cdot 1.3H_2O$ had a platelet morphology with lateral dimensions of submicro/micrometers (Figure S1 of the Supporting Information). After vigorous shaking of the protonated sample in a TBAOH solution (TBA^+/H^+ = 1) for 2 weeks, colloidal TaO_3 nanosheets were

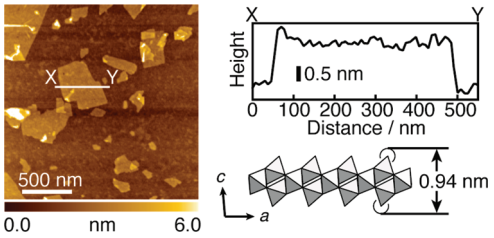

Figure 1. (Left) AFM image of TaO_3 nanosheets deposited on a Si wafer. (Right Top) Height profile along the white line, XY. (Right Bottom) Side view of the crystal structure of the TaO_3 host layer. The hemispheres indicate the oxygen radius.

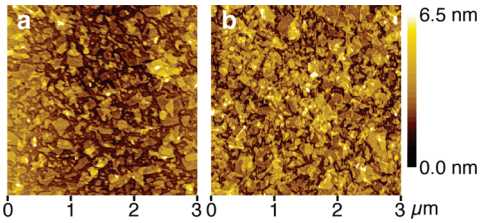

Figure 2. Tapping mode AFM images of the first TaO_3 nanosheet layer on a PDDA-coated Si wafer. Nanosheet concentration: (a) 0.08 and (b) 0.24 g dm^{-3}.

obtained. A typical AFM image of TaO_3 nanosheets adsorbed on a PDDA-precoated Si wafer demonstrates that the nanosheets have a thickness of ~1 nm and a lateral size of several hundred nanometers (Figure 1), being consistent with our previous result. The measured thickness is compatible with the crystallographic thickness, 0.94 nm, of the host layer in $RbTaO_3$,[26] confirming the unilamellar nature of the crystallites.

Construction of Multilayer Films. The TaO_3 nanosheet was deposited on a PDDA-coated Si wafer using the suspension at various concentrations, and the surface coverage of substrate was examined as a function of the concentration in order to obtain a deposited layer of densely tiled nanosheets. The surface coverage increased with the suspension concentration and became saturated at a high concentration. Figure 2 shows AFM images of the first deposited layer of TaO_3 nanosheets at two typical concentrations. The coverage increased from about 60% at the TaO_3 nanosheet concentration ρ = 0.08 g dm^{-3} to about 90% at ρ = 0.24 g dm^{-3}. The overlapped area also increased from about 15 to 45%. The overlapping of nanosheets is inevitable in the deposition of objects having a lateral size of submicrometer range. Some portion of the nanosheets can be adsorbed onto the bare cationic surface, whereas its area may not be large enough to accommodate the whole crystallites.

The TaO_3 nanosheets exhibited intense absorption at a wavelength of 250 nm and below because of its semiconducting nature, whereas PDDA showed negligible absorption in the measured wavelength range of 185−800 nm. The assembly of multilayer film could thus be monitored by UV−vis spectra recorded after each deposition cycle (Figure 3). The nearly linear increment of absorbance at 200 nm indicates that an approximately equal amount of TaO_3 nanosheets was deposited in each cycle, confirming the stepwise growth of multilayer film.

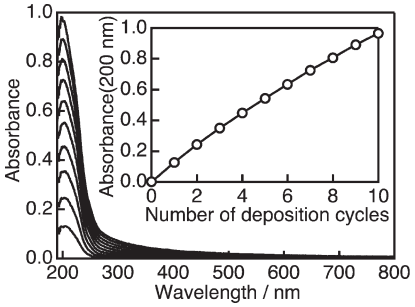

Figure 3. UV−vis absorption spectra in the multilayer buildup process on a quartz glass substrate. The inset shows the dependence of absorbance at 200 nm on the deposition cycle. Note that the absorption is from two films on both sides of the substrate.

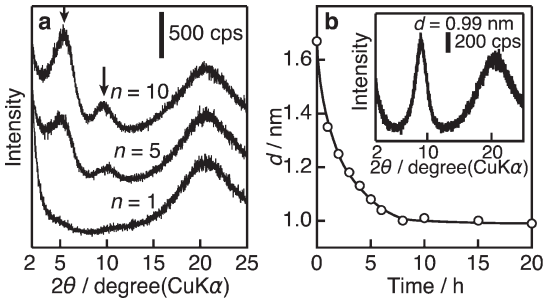

Figure 4. (a) XRD pattern of as-prepared multilayer films of $(PDDA/TaO_3)_n$ with $n = 1$, 5, and 10. Arrows indicate multilayer basal peaks and a broad halo around 20° in 2θ is due to quartz glass substrate. (b) Multilayer repeating distance of $(PDDA/TaO_3)_{10}$ film, d, as a function of UV irradiation time. Inset: XRD pattern for $(PDDA/TaO_3)_{10}$ film after exposure to UV light for 20 h.

The XRD pattern of the obtained films of $(PDDA/TaO_3)_n$ exhibited two diffraction peaks located at $2\theta = 5.3$ and 9.6° (Figure 4a), indicating a repeating periodicity of ~1.7 nm. The evolution of these peaks strongly supports the progressive growth of a nanostructured film composed of repeating $PDDA/TaO_3$ pair. Because the crystallographic thickness of the TaO_3 nanosheet is 0.94 nm, the thickness of the PDDA monolayer is estimated as ~0.7 nm. This value agrees well with those found in the other nanosheet films.[26]

When the $(PDDA/TaO_3)_{10}$ film was exposed to UV light with intensity of 1 mW cm^{-2} at $\lambda < 300$ nm, the multilayer repeating distance contracted continuously with irradiation time down to a constant value of 1 nm (see Figure 4b). The shrinkage upon UV illumination is ascribed to the decomposition of PDDA in the gallery, which is promoted via the photocatalytic activity of the TaO_3 nanosheet. Similar effects have been observed in other multilayer films, such as $PDDA/Ti_{0.91}O_2$ nanosheets[27] and $PDDA/Nb_3O_8$ nanosheets.[28] The final d value of 0.99 nm is close to that of protonated form, $Rb_{0.1}H_{0.9}TaO_3 \cdot 1.3H_2O$, before delamination, indicating the formation of inorganic multilayer structure of TaO_3 sheets accommodating NH_4^+ and H^+ as possible counterions.

(27) (a) Sasaki, T.; Ebina, Y.; Fukuda, K.; Tanaka, T.; Harada, M.; Watanabe, M. *Chem. Mater.* **2002**, *14*, 3524. (b) Shibata, T.; Sakai, N.; Fukuda, K.; Ebina, Y.; Sasaki, T. *Phys. Chem. Chem. Phys.* **2007**, *9*, 2413.

(28) Akatsuka, K.; Takanashi, G.; Ebina, Y.; Sakai, N.; Haga, M.; Sasaki, T. *J. Phys. Chem. Solids* **2008**, *69*, 1288.

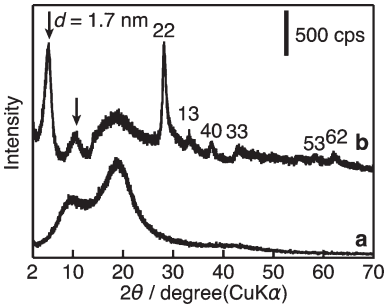

Figure 5. XRD patterns of (a) PS beads and (b) core−shell composites with 10 bilayers of $PDDA/TaO_3$. Arrows indicate XRD peaks with a repeating distance of ~1.7 nm.

Fabrication of Core−Shell Composites and Hollow Spheres. The alternate electrostatic adsorption of PDDA and TaO_3 nanosheets on PS beads produced core−shell composites. XRD pattern of bare PS beads exhibited a broad hump in the range of 10−20° (Figure 5a), which was significantly suppressed after the coating of 10 bilayers of $PDDA/TaO_3$ (Figure 5b). Two peaks located at 2θ values of 5.3 and 10.1° are attributable to the repeating layer pairs of $PDDA/TaO_3$ with a periodicity of ~1.7 nm, analogous to that of multilayer films of $PDDA/TaO_3$. These peaks were enhanced with increasing the number of coating cycles, suggesting the layer-by-layer deposition of PDDA and TaO_3 nanosheet on PS surface. Similar trend has been observed in the shell assembly of $Ti_{0.91}O_2$ nanosheets and MnO_2 nanosheets on polymer spheres.[25] Additional peaks at 28.1, 33.0, 37.3, 42.8, 58.4, and 62.1° could be assigned to reflections of 22, 13, 40, 33, 53, and 62 bands from a two-dimensional, face-centered rectangular unit cell (0.9567 nm × 0.8490 nm) for TaO_3 nanosheet,[26] indicating that the nanosheet architecture remained intact.

The formation of core−shell composites was also confirmed by SEM observation. Figure 6a shows the SEM image of core−shell composites with 10 bilayers of $PDDA/TaO_3$. The spherical shape of the PS particles was preserved after the deposition of $PDDA/TaO_3$, although the surface became rough. In the thermal analysis, the core−shell composites underwent a total weight loss of 82% in two temperature regions (200−300 °C and 350−450 °C) upon heating up to 500 °C, both accompanied by pronounced exothermic peaks due to the combustion of the PS core and PDDA layers (data not shown).

After calcination at 600 °C in air for 4 h, the spherical morphology was still preserved except for a small number of broken spheres in the SEM image (Figure 6b). The TEM image (Figure 6c) further confirmed the hollow nature of the material. Some wrinkles were observed because of the ultrathin shell (expected to be ~10 nm). The SAED pattern (inset in Figure 6c) revealed that the hollow sphere was amorphous. In the corresponding XRD pattern (Figure 7a), no discernible diffraction peaks were observed, further confirming the amorphous state.

The spherical morphology still remained when the calcination temperature rose to 650 °C (Figure 6d and 6e). The diameter of the hollow spheres was about 20% smaller

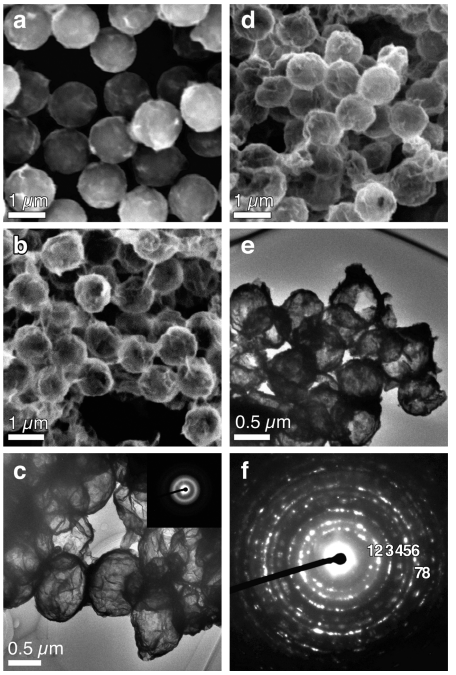

Figure 6. (a) SEM image of core−shell composites with 10 bilayers of PDDA/TaO_3. (b) SEM and (c) TEM images of hollow spheres obtained by calcination at 600 °C. Inset of c shows the corresponding SAED pattern. (d) SEM, (e) TEM, and (f) SAED data of hollow spheres obtained after calcination at 650 °C.

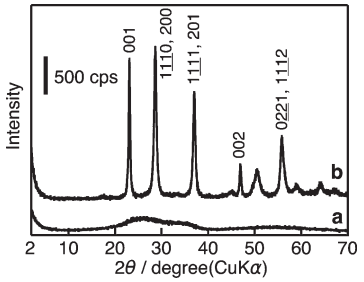

Figure 7. XRD patterns of (a) tantalum oxide hollow spheres prepared through calcination at 600 °C and (b) Ta_2O_5 hollow spheres obtained by calcination at 650 °C.

than that of the original core−shell composites. The SAED pattern of the crystalline phase after calcination at 650 °C was composed of a series of diffraction rings (Figure 6f), and the spacing and indices for rings 1−8 are 0.388 nm (001), 0.315 nm (1$\bar{1}$10), 0.245 nm (1$\bar{1}$11), 0.195 nm (002), 0.180 nm (2$\bar{1}$51), 0.166 nm (11$\bar{1}$2), 0.157 nm (22$\bar{2}$0) and 0.146 nm (22$\bar{2}$1), respectively, being consistent with the orthorhombic Ta_2O_5 phase (JCPDS, No. 25−0922). A HRTEM image of the hollow sphere obtained after calcination at 650 °C (see Figure S2 in the Supporting Information) showed the fringe with lattice spacing of 0.388 nm corresponding to (001) of orthorhombic Ta_2O_5. In addition, XRD data (Figure 7b) also support the formation of orthorhombic Ta_2O_5.

Very recently, Agrawal et al.[8] reported the synthesis of a Ta_2O_5 capsule through the surface precipitation of Ta_2O_5 on β-diketone-functionalized PS beads. However, the shell thickness (115−400 nm) was much larger than that in the present work. Although the same orthorhombic Ta_2O_5 hollow sphere was formed at the same calcination temperature, the

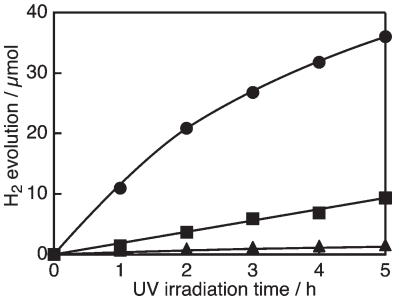

Figure 8. Time course of hydrogen evolution over Ta_2O_5 hollow spheres (●); amorphous hollow spheres (■); commercial Ta_2O_5 powder (▲). Reaction conditions: 1 mg of catalyst, 2 cm^3 of aqueous 10 vol % methanol solution.

XRD pattern showed that an amorphous phase was definitely present in their sample. Agrawal et al. considered that organic residue in the composite particles hindered the coagulation of Ta_2O_5 nanoparticles and affected the crystallization of Ta_2O_5. On the other hand, in our system, the ultrathin shell thickness and regularly layered adsorption of TaO_3 nanosheets in the shell are favorable for the total crystallization of Ta_2O_5.

Photocatalytic Water Splitting. The photocatalytic activity of the hollow spheres was examined for hydrogen evolution from an aqueous 10 vol % methanol solution under UV irradiation. Figure 8 shows that the amount of evolved H_2 gas increased nearly in a linear fashion with the irradiation time.[29] The rate of H_2 generation over amorphous hollow spheres was 1.6 μmol h^{-1}, whereas that on commercial Ta_2O_5 powder under the same conditions was very limited (0.3 μmol h^{-1}). Surprisingly, the Ta_2O_5 hollow spheres showed remarkably good photocatalytic activity at a rate of 7.1 μmol h^{-1}. This is 4 times and 20 times greater than that generated on amorphous hollow spheres and commercial Ta_2O_5 powder, respectively. The enhancement in photocatalytic activity with respect to Ta_2O_5 powder is significantly high compared with those reported previously.[3] It has been reported that mesoporous Ta_2O_5 also shows high photocatalytic activity.[5−7] Ta_2O_5 in mesoporous structure and that in a morphology of hollow microsphere have common features in terms of large surface area, high crystallinity, and ultrathin nature, which are advantageous as a photocatalyst. One distinct point between these materials may be nano/microstructures. The former material is composed of narrow channels, which may not be advantageous for migration of reactant and product molecules to reaction sites. In contrast, reaction sites on the hollow microsphere are exposed to open environments where the molecules should be freely accessible.

With the irradiation of UV light and subsequent excitation of tantalum oxide, a multitude of electron/hole pairs will be generated.[5] Two main parameters generally govern the photocatalytic activity. One is the surface area, which controls the amount of surface active sites for undertaking reaction, and the other is the crystallinity, which

(29) There is some deviation from the linearity, which may possibly be due to suppressing effect by the evolved gas, a change in pH, and so on. The H_2 evolution rate over the reaction course was estimated by assuming the linear relationship.

influences the recombination probability of electrons and positive holes. We measured the specific surface area of the catalysts using the multipoint Brunauer−Emmett−Teller (BET) method. S_{BET} was 47 and 39 $m^2 g^{-1}$ for amorphous and crystallized (Ta_2O_5) hollow spheres, respectively. These values are considerably larger than S_{BET} of 1.7 $m^2 g^{-1}$ for the commercial Ta_2O_5 powder. Although an amorphous hollow sphere had a slightly higher surface area, it may have more surface defects because of its amorphous nature, which will result in a higher recombination rate of electrons and holes. The number of surface defects is expected to decrease upon crystallization. High crystallinity ensures the efficient migration of electrons and holes through the lattice to the surface. Thus, crystallized hollow spheres show considerable enhancement of photocatalytic activity. Noda et al. also found that the photocatalytic activity of the NiO_x-loaded mesoporous Ta_2O_5 for overall water splitting was improved by conversion from amorphous to crystalline state.[6] On the other hand, the considerably low photocatalytic activity of commercial Ta_2O_5 powder is due to the very low surface area. Therefore, the photocatalyst such as the Ta_2O_5 hollow spheres reported here, having both high crystallinity and sufficient S_{BET}, exhibits higher photocatalytic activity.

Conclusions

We have demonstrated the successful fabrication of multilayer films and hollow spheres via sequential adsorption assembly of TaO_3 nanosheets and PDDA polycation. TaO_3 ultrathin film was proven to have high photocatalytic activity for decomposition of organic species under UV irradiation. Ta_2O_5 hollow spheres showed remarkably effective photocatalytic properties for hydrogen evolution from an aqueous methanol solution upon exposure to UV light irradiation. The rate of hydrogen generation over Ta_2O_5 hollow spheres exceeded 20 times that of commercial Ta_2O_5 powder.

Because photocatalytic overall water splitting is frequently promoted by loading an appropriate cocatalyst, we intend to further investigate the photocatalytic activity of Ta_2O_5 hollow spheres loaded with various cocatalysts.

Acknowledgment. This work was partly supported by the World Premier International Research Center (WPI) Initiative on Materials Nanoarchitectonics, MEXT, and CREST of the Japan Science and Technology Agency (JST). Financial support extended to J.H.H. from the China Scholarship Council is gratefully acknowledged.

Supporting Information Available: (i) SEM images of $RbTaO_3$ and $Rb_{0.1}H_{0.9}TaO_3 \cdot 1.3H_2O$ and (ii) HRTEM image and SAED pattern of hollow spheres obtained via calcination at 650 °C (PDF). This material is available free of charge via the Internet at http://pubs.acs.org.